# Influence of Chemical Modeling on URANS Simulations of Longitudinal Thermoacoustic Instability

Alex Falco\*†, Alessandro Montanari\*, Marco Grossi\*, Paolo Maria Zolla\*, Francesco Nasuti\*

\*Sapienza University of Rome

Via Eudossiana 18, 00184, Rome, Italy

alex.falco@uniroma1.it · alessandro.montanari@uniroma1.it · marco.grossi@uniroma1.it

paolomaria.zolla@uniroma1.it · francesco.nasuti@uniroma1.it

Corresponding author

## **Abstract**

This study investigates the impact of ignition delay modeling on the prediction of thermoacoustic instabilities using a two-dimensional axisymmetric Unsteady Reynolds-Averaged Navier-Stokes approach. The Continuously Variable Resonance Combustor, a well-documented test case known for exhibiting longitudinal combustion instability, is used as reference for this analysis. After assessing the primary role of ignition delay in the numerical prediction of thermoacoustic instabilities, a set of simplified one-step oxymethane chemical mechanisms, each calibrated to represent different ignition delays, is examined. The study focuses on identifying how variations in ignition delay influence key observables of combustion instability, specifically the amplitude and frequency of pressure oscillations in the resulting limit cycle. The main objective is to show how physics-based assumptions in chemical modeling can improve the accuracy of predictions and lead to better agreement with experimental results.

# 1. Introduction

Combustion Instability (CI) is a critical phenomenon that can severely hinder the final stages of Liquid Rocket Engine (LRE) development. CI manifests as self-sustained pressure oscillations with a well-defined spectrum and peak-to-peak amplitudes exceeding 10% of the mean chamber pressure. The most detrimental form of the phenomenon is high-frequency CI (typically above 1 kHz), often referred to as "screaming". Originating from a complex feedback mechanism involving acoustic waves, hydrodynamics, and unsteady heat release interacting with the natural acoustic modes of the combustion chamber, this type of instability is thus commonly known as "thermoacoustic". The resulting large-amplitude, high-frequency oscillations are difficult to predict during the design phase of an LRE and can lead to catastrophic thermal and structural failures. Although the costly development of the Rocketdyne F-1 engine first drew significant attention to this phenomenon in the late 1950s, the complex interplay of the underlying physical processes has continued to make high-frequency combustion instability difficult to fully understand to this day. As a result, efforts to prevent or mitigate it remain incomplete. Continued research is therefore essential to deepen our understanding and to develop reliable predictive tools that can support the design of modern liquid rocket engines.

Nowadays, high-frequency CI is investigated through a synergistic approach that combines lab-scale experiments with a hierarchy of numerical modeling techniques. Lab-scale combustors offer a valid cost-effective alternative to expensive full-scale tests. These experiments serve as valuable tools for analyzing key engine features that can be preserved in smaller scales, while also playing a crucial role in the calibration and validation of computational models. A significant contribution to the field comes from extensive test campaigns involving the Continuously Variable Resonance Combustor (CVRC)<sup>3–5</sup> at Zucrow Labs, Purdue University, where the influence of the engine geometric features on combustion instability has been thoroughly addressed, identifying the injector-chamber design as one of the primary factors driving instability. In this regard, shear-coaxial injectors, commonly used in liquid oxygen/methane (LOX/CH<sub>4</sub>) and liquid oxygen/hydrogen (LOX/H<sub>2</sub>) propulsion systems, have shown notable susceptibility to the phenomenon. As demonstrated by the CVRC studies,<sup>3–5</sup> this sensitivity is strongly influenced by the longitudinal acoustic spectrum of the oxidizer post and its strict relationship with the heat release rate spectrum,<sup>6</sup> suggesting a modulation of unsteady combustion by axial pressure waves propagating within the injectors. Other lab-scale combustors, purposefully designed or used for studying combustion instabilities, include the TIC combustor,<sup>7</sup> also at Purdue University, and the BKN,<sup>8</sup> BKH,<sup>9</sup> and BKD<sup>6</sup> combustors at DLR, The German Aerospace Center, in Lampoldshausen, Germany. It is important to note that, since experimental data typically consist primarily of pressure measurements at key locations

within the combustor, a detailed phenomenological understanding can only be achieved through high-fidelity numerical simulations, which are instead able to highlight key flow features.

High-fidelity computational fluid dynamics (CFD) approaches, such as Large Eddy Simulations (LES), Detached Eddy Simulations (DES), and even Unsteady Reynolds Averaged Navier-Stokes (URANS) simulations have significantly advanced the understanding of the physical mechanisms driving high-frequency combustion instability. 10-14 In particular, results from Harvazinski et al. 10 revealed a potential coupling mechanism involving the interaction between propellant injection and pressure oscillations within recessed shear-coaxial injectors. These injectors can exhibit cyclic accumulation and release of fuel from the fuel sleeves, a behavior driven by their unique geometric and acoustic characteristics. According to these findings, a possible feedback mechanism can thus be described as follows: since shear coaxial injectors are designed with coaxial streams of fuel and oxidizer, in the region where the two propellants interact, also known as the "recess", a shear layer forms along its entire length, featuring a strong radial density gradient that promotes mixing. When pressure oscillations are present in the combustion chamber, acoustic waves may enter the injector recess traveling along the longitudinal direction, resulting in a longitudinal pressure gradient. The interaction between orthogonal density and pressure gradients generates baroclinic torque, producing vorticity at the propellant interface. Strong upstream-traveling shocks can bend the fuel-oxidizer boundary toward the less dense fluid, usually the fuel, temporarily interrupting or slowing down fuel injection and forming fuel-rich vortices. This phenomenon causes the combustion to locally stall. Similarly, downstream-traveling waves, either shocks or expansions, can push these vortices and the trapped fuel toward the flame. The sudden combustion of these released fuel pockets then produces a peak in heat release. These fluctuations in heat release generate new pressure oscillations, potentially closing a thermoacoustic feedback loop. If the acoustic environment of the chamber allows the timing of these key events within the feedback loop to align with the chamber natural frequencies, resonance occurs, leading to self-excited high-frequency combustion instability. A schematic representation of this behavior is shown in Figure 1.

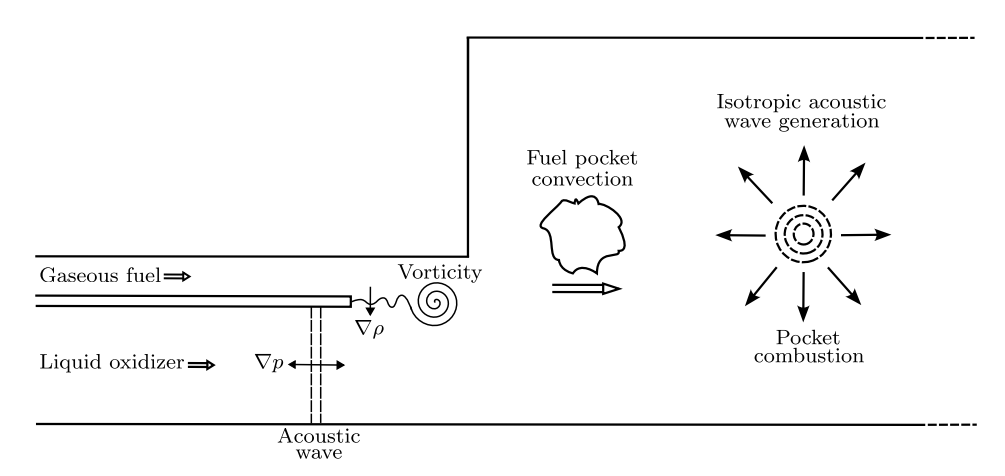


Figure 1: Possible feedback dynamics of shear coaxial injectors.

Although valuable for advancing our understanding of combustion instability and its underlying mechanisms, both lab-scale experiments and high-fidelity simulations have limitations when it comes to supporting iterative LRE design processes. Lab-scale engine configurations, while informative, cannot definitively predict whether combustion instability will occur at full-scale, as the phenomenon is highly sensitive to engine size. High-fidelity simulations, on the other hand, are not well-suited for iterative design due to their substantial computational cost, which scales with the level of fidelity required. Thus, to support practical design efforts, research has increasingly turned toward low-order models. 15,16 This numerical approach is based on a highly simplified physical modeling, retaining only the essential processes that govern combustor instability dynamics. The objective is not to capture detailed flow structures, but rather to provide a rapid assessment of chamber stability. However, such simplifications may neglect important aspects of thermoacoustic behavior. To compensate for these limitations, a coupling mechanism is introduced via a submodel, commonly referred to as "response function" (RF). It is clear that the predictive accuracy of low-order models strongly depends on the formulation of this submodel. Several response functions formulations exist in the literature, among which one of the most widely adopted is the  $n-\tau$  model, based on Crocco's time-lag theory, <sup>17</sup> which establishes a direct relationship between pressure and heat release oscillations, shifted through a space/time lag. When properly tuned, the n- $\tau$  model has shown good predictive capabilities in capturing the onset and characteristics of combustion instability. <sup>18</sup> In the literature, a direct link between pressure and heat release, such as in this case, is usually established, bypassing the physical causality between the two variables through the use of model parameters which are often derived and calibrated using data from high-fidelity simulations or experiments. This use of external data, however, limits the predictive capabilities and range of application of the low-order approach. A more physically informed response function is the one developed by D'Alessandro et al., <sup>19</sup> which replicates the previously described behavior of shear coaxial injectors by linking pressure fluctuations in the recess to unsteady fuel mass flow rate. This indirect closure of the feedback loop introduces a possible cause-effect relationship between acoustic waves and heat release fluctuations, allowing the response function to operate without the need for external calibration data and thereby enhancing its predictive capability and general applicability. This method has proven effective in capturing both longitudinal and transverse instabilities within ideal and real-fluid Eulerian frameworks, across both single- and multi-injector engine configurations. <sup>19–24</sup> Nonetheless, model parameters are still employed to simplify complex physical phenomena, such as in the chemical modeling to avoid the stiffness of detailed mechanisms. A clearer characterization of these parameters, along with a physically informed approach to selecting them, would be highly beneficial.

In this scenario, the present work aims to exploit Unsteady Reynolds Averaged Navier-Stokes simulations to support the development of more physically informed simplifications for modeling combustion instabilities in low-order approaches, while maintaining affordable computational costs. A key objective is to improve understanding of how combustion model parameters, specifically ignition delay, affect instability predictions. This insight could help isolate the essential mechanisms required for low-order models to improve their predictive capabilities and could help inform the tuning of global combustion models. Moreover, such insights are valuable for high-fidelity CFD as well. Understanding the impact of combustion modeling on instability predictions enables a more informed selection of chemical mechanisms best suited to the specific operating conditions under investigation. The study investigates the influence of ignition delay modeling on the predicted oscillation frequency and amplitude of the CVRC test case, evaluates the limitations of current models, and demonstrates how small adjustments can enable even simplified approaches to reasonably capture combustion instability behavior.

# 2. Numerical Model

The numerical analysis of combustion instability requires accurate modeling of convective, acoustic, and diffusive phenomena. The presence of heterogeneous and complex physical mechanisms, combined with the need for time-accurate solutions due to the inherently unsteady nature of the phenomenon, poses a significant challenge for numerical solvers. To address these complexities within a computationally feasible framework, simulations were carried out by solving the unsteady Reynolds-Averaged Navier–Stokes equations for a compressible, single-phase, multi-component mixture of reacting thermally perfect gases. The model incorporates variable thermodynamic and transport properties and is implemented using an in-house solver. The governing equations are presented below:

$$\frac{\partial(\rho y_i)}{\partial t} + \nabla \cdot (\rho y_i \mathbf{v}) = -\nabla \cdot \mathbf{j}_i + \dot{\omega}_i \quad (i = 1, ..., N_s)$$
 (1a)

$$\frac{\partial(\rho \mathbf{v})}{\partial t} + \nabla \cdot (\rho \mathbf{v} \mathbf{v}) = \nabla \cdot \mathbf{S}$$
 (1b)

$$\frac{\partial(\rho e_0)}{\partial t} + \nabla \cdot (\rho e_0 \mathbf{v}) = \nabla \cdot (\mathbf{v} \cdot \mathbf{S}) - \nabla \cdot \mathbf{q}$$
(1c)

where  $\rho$ ,  $y_i$ , t,  $N_s$ , and  $\mathbf{v}$  denote, respectively, the density of the mixture, the mass fraction of the i-th species, the time variable, the total number of species, and the velocity vector. The mixture total energy per unit mass,  $e_0$ , is defined as:

$$e_0 = \sum_{i=1}^{N_s} y_i (e_i + \Delta e_{f,i}^0) + \frac{\mathbf{v} \cdot \mathbf{v}}{2}$$
 (2)

where  $e_i$  is the internal energy of the *i*-th species. On the right hand side of Eqs. (1), the quantities with the divergence operator,  $(\nabla \cdot)$ , can be expressed as:

$$\mathbf{j}_{i} = -\left(\frac{\mu}{\mathrm{Sc}} + \frac{\mu_{\mathrm{t}}}{\mathrm{Sc}_{\mathrm{t}}}\right) \nabla y_{i} \tag{3}$$

$$\mathbf{S} = -p\mathbf{I} - (\mu + \mu_{t}) \left\{ \frac{2}{3} (\nabla \cdot \mathbf{v}) \mathbf{I} + \left[ \nabla \mathbf{v} + (\nabla \mathbf{v})^{\mathrm{T}} \right] \right\}$$
(4)

$$\mathbf{q} = -\left(k + \frac{\mu_{i}}{Pr_{i}} \sum_{i=1}^{N_{s}} y_{i} c_{p,i}\right) + \sum_{i=1}^{N_{s}} \left(h_{i} + \Delta h_{f,i}^{0}\right) \mathbf{j}_{i}$$
 (5)

which represent the mass diffusion flux vector of the *i*-th species, the stress tensor, and the heat flux vector, respectively. Note that the mass fluxes  $\mathbf{j}_i$  are corrected to ensure that they sum to zero by distributing the residual according to the

species mass fraction.<sup>25</sup> The terms  $\mu$  and k denote the molecular viscosity and thermal conductivity, respectively, while the terms  $\mu_t$  and  $k_t$  the corresponding eddy (or turbulent) counterpart.

Thermodynamic closure is obtained assuming a thermally perfect gas mixture, governed by the ideal equation of state:

$$p = \rho RT \quad \text{with} \quad R = \sum_{i=1}^{N_s} y_i R_i \tag{6}$$

where p, T, and  $R_i$  denote, respectively, pressure, temperature, and the i-th species gas constant. The caloric equation of state is obtained expressing the constant pressure specific heats  $c_{\mathrm{p},i}$  as functions of temperature using seventh-order polynomial fits for each species, taken from Gordon et al.<sup>26</sup> From the same chemical database, the standard formation enthalpy  $\Delta h_{\mathrm{f},i}^0$  is also retrieved. The molecular transport properties,  $\mu$  and k, for each species are approximated by fourth-order polynomials of temperature,<sup>26</sup> with the mixture properties computed using Wilke's rule. Species diffusion is considered to be the same for all the species through a constant Schmidt number assumed equal to  $\mathrm{Sc}=1.0$ . Turbulent viscosity  $\mu_{\mathrm{t}}$  is modeled using the Spalart–Allmaras one-equation model,<sup>27</sup> chosen for its low computational cost. The turbulent thermal conductivity  $k_{\mathrm{t}}$  is computed based on a constant turbulent Prandtl number  $\mathrm{Pr}_{\mathrm{t}}=0.9$ , while the turbulent Schmidt number  $\mathrm{Sc}_{\mathrm{t}}$  is also assumed constant and set to 0.9.

The chemical source terms  $\dot{\omega}_i$  in Eq. (1a) are computed as the sum of contributions from each of the  $N_r$  reactions in the selected chemical mechanism, given by:

$$\dot{\omega}_{i} = \mathcal{M}_{i} \sum_{j=1}^{N_{r}} \left( v_{i,j}^{P} - v_{i,j}^{R} \right) \left[ K_{f,j} \prod_{s=1}^{N_{s}} \left( \frac{\rho_{s}}{\mathcal{M}_{s}} \right)^{v_{s,j}^{R}} - K_{b,j} \prod_{s=1}^{N_{s}} \left( \frac{\rho_{s}}{\mathcal{M}_{s}} \right)^{v_{s,j}^{P}} \right]$$
(7)

where a generic reaction involving species  $\mathcal{B}_i$  is expressed using stoichiometric coefficients for reactants  $v_{i,j}^{R}$  and products  $v_{i,j}^{P}$ , as:

$$\sum_{i=1}^{N_{s}} v_{i,j}^{R} \mathcal{B}_{i} \rightleftharpoons \sum_{i=1}^{N_{s}} v_{i,j}^{P} \mathcal{B}_{i} \quad (j = 1, ..., N_{r})$$
(8)

Here,  $K_{f,j}$  and  $K_{b,j}$  denote the forward and backward reaction rates of the *j*-th reaction, respectively, and are related through the equilibrium constant  $K_j$  by  $K_{b,j} = K_{f,j}/K_j$ . Note that for reactions modeled as irreversible (forward only), the backward rate  $K_{b,j}$  is set to zero.

The solver employs a second-order accurate finite-volume scheme in both time and space. Specifically, second-order accuracy in space is achieved through a piece-wise linear Godunov-like approach. Both convective and diffusive terms are integrated in time by a second-order Runge-Kutta scheme. The solution is upwinded by the HLLC approximate Riemann solver in the formulation by Batten et al.<sup>28</sup> To explicitly integrate stiff chemical kinetics, a Strang-splitting approach is employed.

# 3. Experimental and Computational Setup

As stated in the previous section, the benchmark test case for this parametric study is the Continuously Variable Resonance Combustor (CVRC), a well-established lab-scale apparatus featuring a single shear coaxial injector and exhibiting longitudinal combustion instability. A distinctive feature of the CVRC is its ability to vary the length of the oxidizer post, enabling a wide range of configurations to be tested within a single firing.<sup>3</sup> This flexibility makes the CVRC particularly well-suited for investigating the influence of oxidizer-post length on combustion stability, providing a comprehensive dataset available in the open literature. For the purposes of this study, this test case was selected because of its simplicity, which allows for a computationally efficient domain reduction using a 2D axisymmetric approximation, while also enabling a detailed investigation of the underlying flow dynamics.

The CVRC features a 38.1 cm long combustion chamber, connected to a short convergent-divergent nozzle. The oxidizer post can be actuated in order to achieve an injector length between 8.89 cm and 19.05 cm. A fully gaseous injection is employed. Specifically, the oxidizer comprises a mixture of  $H_2O$  and  $O_2$  resulting from the decomposition of hydrogen peroxide ( $H_2O_2$ , 90% weight in water), injected at a relatively high temperature injection of 1030 K, while the fuel is methane ( $CH_4$ ), injected at a temperature of 300 K. Well-defined boundary conditions at the oxidizer post are achieved using a choked inlet, which acoustically isolates the injector from the injection dome. The relevant experimental parameters are summarized in Table 1, while a detailed description of the experimental apparatus can be found in Yu et al.<sup>3</sup> The unstable configuration selected for this analysis features an injection length of 13.9 cm and is commonly referred to as the Medium Post Configuration (MPC).

The boundary conditions applied in the numerical simulations are illustrated in Fig. 2. The boundary labels shown in the figure correspond to the following implementations:

Table 1: Ge	cometrical data of t	he CVRC experimenta	l setup and details of the	e investigated load points. <sup>3</sup>
Tuoic 1. Oc	omenical data of t	ine e vite experimenta		

Parameter	Data
Oxidizer mass flow rate, kg/s	0.320
Oxidizer H <sub>2</sub> O mass fraction	57.6%
Oxidizer O <sub>2</sub> mass fraction	42.4%
Oxidizer temperature, K	1030
Fuel mass flow rate, kg/s	0.027
Fuel CH <sub>4</sub> mass fraction	100%
Fuel temperature, K	300
Mixture ratio	11.85
Throat diameter, cm	2.08
Chamber length, cm	38.10
Chamber diameter, cm	4.50
Oxidizer post diameter, cm	2.05

- *Inflow*: implemented at the left bound of the fuel annulus and of the oxidizer post inlet. These boundary conditions prescribe a fixed mass flux and total temperature.
- Walls: adiabatic, no-slip viscous wall boundaries.
- Symmetry: enforces axial symmetry, treated numerically as an Eulerian wall.
- Outflow: applies a zero-gradient extrapolation for all flow variables at the boundary.
- Rotational Symmetry: treated as an Eulerian wall while accounting for the rotational symmetry of the domain around the axis.

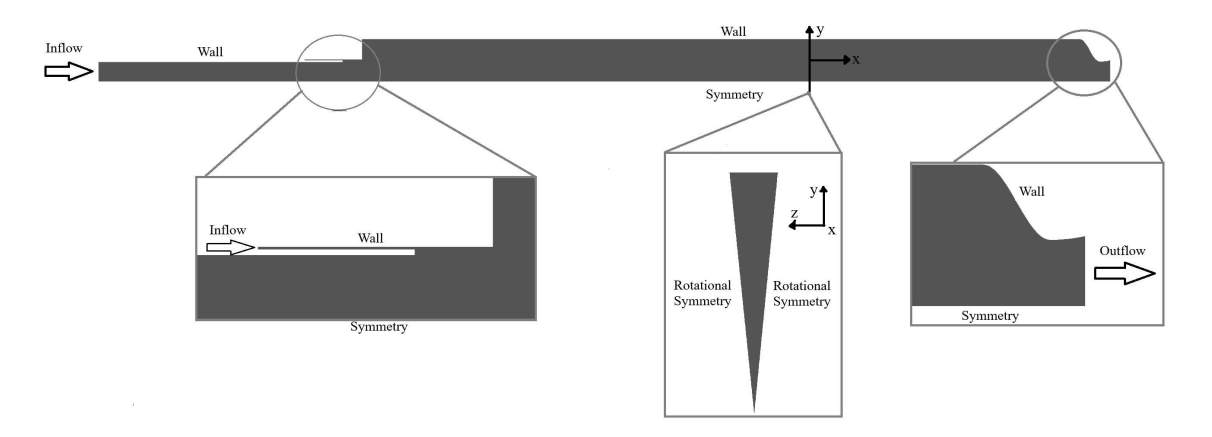


Figure 2: Computational domain and boundary conditions.

The domain is discretized using a multi-block structured mesh comprising 23000 cells, as shown in Fig. 3. A key aspect of the mesh design is the targeted refinement applied to critical flow regions. In particular, the recess and injection plate shear layers are finely resolved, given their central role in the development of the thermoacoustic feedback loop through the cyclic accumulation and release of fuel pockets, previously described in Section §1. To maintain computational efficiency, however, a more conservative refinement strategy is applied elsewhere. As shown in the zoomed view of the nozzle region, the mesh within the combustion chamber remains relatively uniform, with localized refinement only near walls to capture boundary-layer effects. Additional refinement is introduced at the nozzle throat to properly resolve the nozzle—acoustic interactions, which are essential to the longitudinal dynamics under investigation. The system is initialized with a slightly perturbed near-steady-state field.

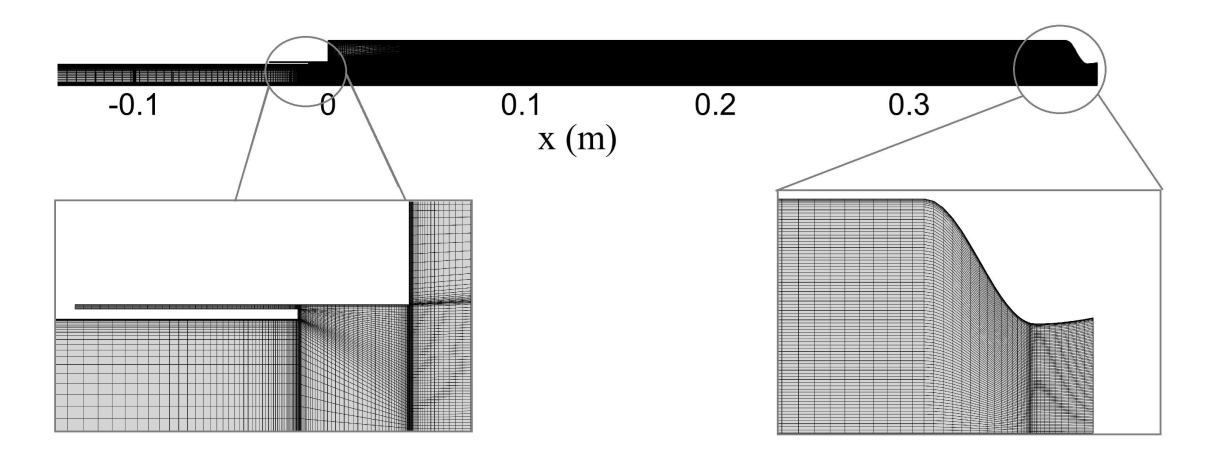


Figure 3: Computational grid.

### 3.1 Role of Chemical Modeling in Thermoacoustic Instability

In combustion instability studies, it is common practice to use simplified combustion models, <sup>10–12,29,30</sup> such as global or skeletal mechanisms, not only because of the prohibitive complexity and stiffness of detailed mechanisms, but also due to a prevailing preference for incorporating more sophisticated turbulence models over detailed chemical fidelity, essential for accurately capturing complex turbulent-acoustic-flame interactions. However, while these simplified models often provide satisfactory predictions of key flow properties such as temperature, composition, and heat release rate, they may fail to capture the unstable behavior associated with thermoacoustic coupling.

To illustrate this, two chemical models have been considered for the present study: the Westbrook-Dryer (WD) model with Andersen correction,<sup>31</sup> which is a two-step global mechanism featuring 5 species and 2 reactions, and the John-Lindstedt Recombination (JLR) mechanism,<sup>32</sup> which is a global multi-step model featuring 9 species and 7 reactions. The simulation results are presented in Fig. 4, showing the pressure signal sampled near the faceplate, along with the corresponding temperature distributions at the first and second pressure maxima and minima. Although more complex and detailed, the JLR model fails to capture the self-excited nature of combustion instability, while the simpler WD-Andersen model successfully reproduces it. Specifically, as shown in Figs. 4(i) and 4(j), the WD-Andersen model predicts pronounced pressure oscillations with a dominant frequency of 1545 Hz, in agreement with earlier works, 10,33 and maintains a steady oscillation amplitude. In contrast, the JLR model exhibits significant damping, with the pressure oscillations gradually decreasing towards the expected steady-state value of 15.8 bar. The comparison of temperature distributions in Fig. 4 reveals a key phenomenological difference between the two chemical mechanisms, which might explain the damping observed in the JLR case. Specifically, the presence of a fully ignited oxidizer-fuel interface extending into the recess region in the JLR case appears to disrupt a crucial driver of combustion instability, namely the cyclic accumulation and release of injected fuel. This unsteady process plays a key role in the onset of instabilities, as it involves the periodic extinction and reignition of the flame, thereby generating acoustic waves that may couple with the chamber natural frequencies. In the JLR case, however, as the flame propagates into the recess, as shown in Fig. 4(h), it effectively separates the fuel and oxidizer streams with a layer of combustion products, reducing local density gradients and thereby weakening the local baroclinic torque. This reduction in baroclinic vorticity disrupts the cyclic accumulation and release of fuel pockets that, in this test case, sustains the instability mechanism.

The primary difference between the employed chemical models that may explain the observed discrepancy in combustion instability predictions lies in their ignition delay. It is reasonable to focus on modeling parameters related to chemical timescales, as combustion instability is inherently an unsteady phenomenon. Moreover, since the dynamics of combustion instability depends, among other factors, on the space/time lag between acoustic perturbations and unsteady heat release, as originally proposed by Crocco's time lag theory, <sup>17</sup> ignition delay emerges as a key parameter. In this regard, existing literature offers insightful discussions on the role of chemical modeling in predicting combustion instability. A key contribution relevant to the objectives of this paper is the work by Sardeshmukh et al. <sup>34</sup> Their work compares the behavior of a detailed mechanism (GRI-1.2) with that of a one-step global combustion model. Their study highlights how the simplified model significantly underestimates the ignition delay compared to the detailed mechanism. This underestimation leads to a higher predicted limit cycle frequency and notable discrepancies in oscillation amplitude in simulations of the CVRC test case. While this comparison is informative, the significant differences in the level of chemical mechanism detail prevent isolating the effects of ignition delay on thermoacoustic predictions. This

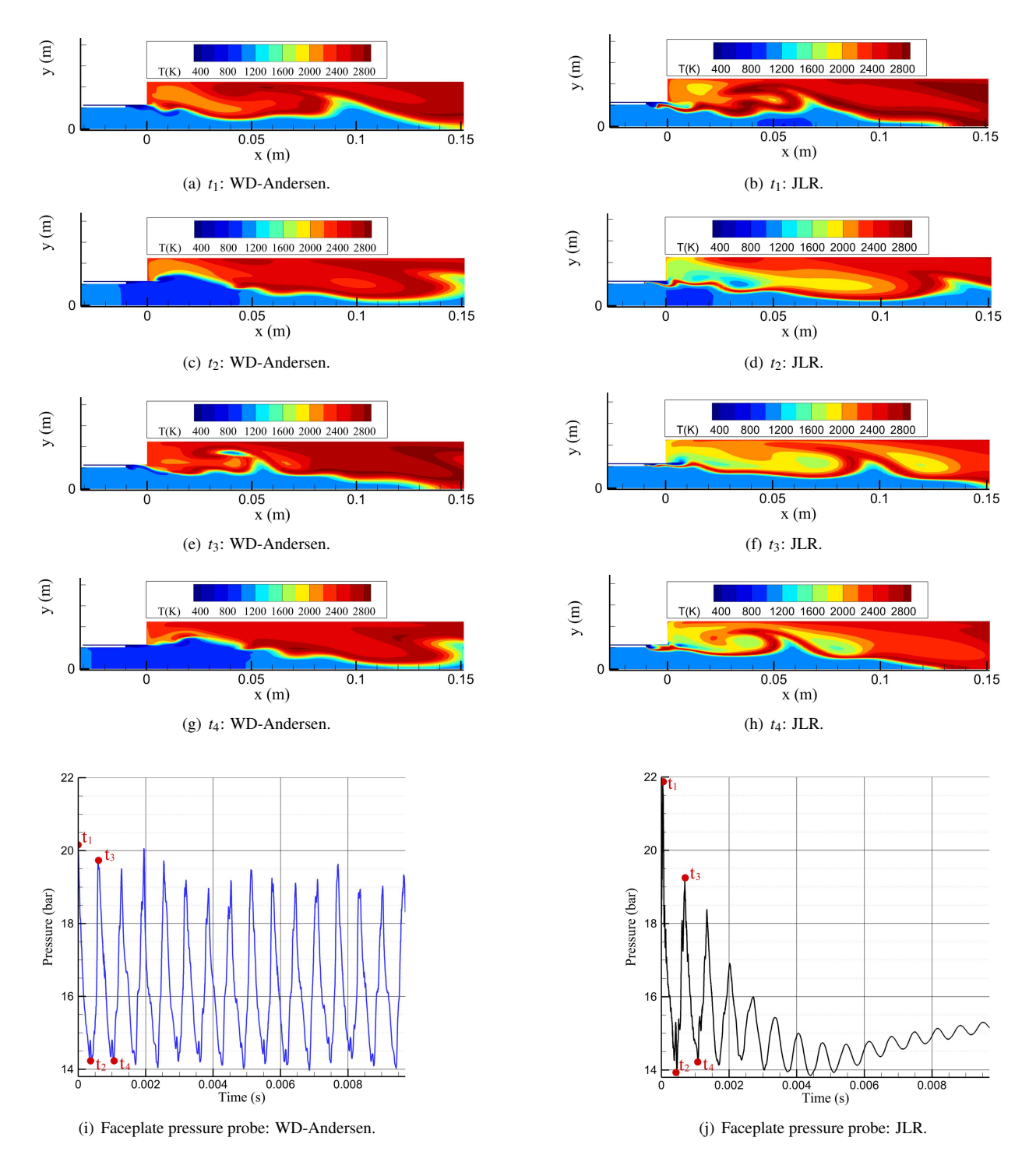


Figure 4: Comparison of results obtained with the WD-Andersen and the JLR chemical models (equal tick spacing on *x* and *y* axes for the temperature distributions).

motivates the present study to conduct a more focused investigation into how ignition delay, as predicted by comparably detailed models, affects combustion instability predictions.

To evaluate the ignition delay predicted by various chemical models, an in-house batch reactor solver has been employed using libraries available in the Cantera software.<sup>35</sup> The initial conditions for the batch reactor tests correspond to those of the CVRC test case, featuring the propellant mixture detailed in Table 1 and a chamber pressure of 15.8 bar. In this context, the ignition delay is defined as the time required for a given mixture, at a specified initial pressure, to experience a temperature increase of 300 K above its initial temperature. To establish physically

meaningful reference values, two detailed chemical mechanisms have been considered, namely the DTU and FFCM-2 mechanisms. The DTU mechanism,<sup>36</sup> developed by the Technical University of Denmark, includes 68 species and 631 reactions, while the FFCM-2 (Foundational Fuel Chemistry Model),<sup>37</sup> developed at Stanford University, comprises 96 species and 1054 reactions. Both mechanisms are highly detailed and computationally demanding, serving primarily as physical benchmarks rather than practical models for CFD simulations.

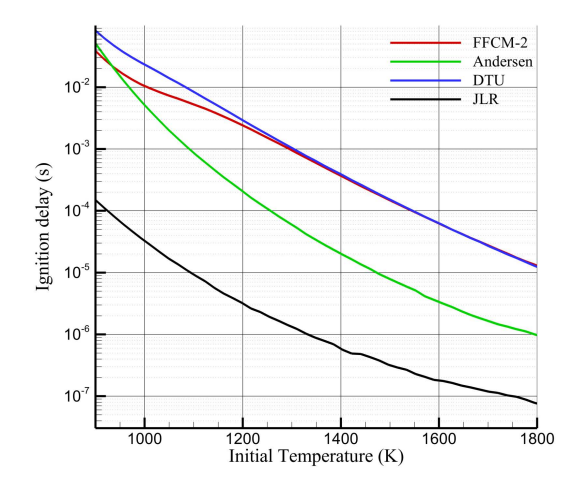


Figure 5: Predicted ignition delay from batch reactor simulations for different chemical mechanisms.

Results are presented in Fig. 5, showing the ignition delay as a function of the initial propellant temperature for the DTU, FFCM-2, JLR, and WD-Andersen chemical mechanisms. Note that the ignition delay curves for the DTU and FFCM-2 chemical models overlap across a wide range of initial propellant temperatures, indicating that they can be considered reliable references for physically realistic ignition delay values. The significant differences in ignition delay observed between the WD-Andersen and JLR mechanisms in Fig. 5 support the earlier hypothesis that ignition delay plays a crucial role in the differing combustion dynamics exhibited by the two models, previously seen in Fig. 4. Although both models show significant discrepancies from the reference data, consistently underestimating the ignition delay, the extent of this underestimation is substantially different. The JLR model exhibits deviations of two to three orders of magnitude, whereas the WD-Andersen model underestimates the ignition delay by roughly one order of magnitude, providing a closer match to the expected ignition dynamics. The very short ignition delay predicted by the JLR model may explain the behavior seen in Fig. 4, where rapid flame ignition inside the recess disrupts the fuel accumulation and release dynamics. In contrast, the WD-Andersen model predicts a dominant frequency of 1545 Hz, 10,33 overestimating the experimental value which is approximately 1327 Hz. This discrepancy has been partially attributed in the literature to adiabatic wall boundary conditions, 10 but may also result from the model underprediction of ignition delay. Indeed, a shorter ignition delay reduces the space/time lag between acoustic perturbations and unsteady heat release, potentially increasing the system resonant frequency by accelerating the thermoacoustic feedback loop dynamics. These observations highlight the critical role of chemical time scales, specifically ignition delay in this case, in combustion instability dynamics, emphasizing the need for appropriate physical fidelity even when using reduced-order frameworks.

For this purpose, a simplified global one-step mechanism, referred to as "OSK" is derived from the WD-Andersen model. The full set of reactions and corresponding parameters for the original WD-Andersen mechanism is reported in Table 2, where A,  $\beta$ , and  $E_a$  denote the pre-exponential factor, temperature exponent, and molar activation energy, respectively. These parameters define the forward reaction rate  $K_f$  of the j-th reaction (previously introduced in Eq. (7)), which is expressed following the Arrhenius equation as:

$$K_{\rm f}(T) = A \cdot T^{\beta} \cdot \exp\left(-\frac{E_{\rm a}}{\mathcal{R}T}\right)$$
 (9)

with  $\mathcal{R}$  being the universal gas constant. The OSK mechanism is constructed by isolating the first reaction of the WD-Andersen model, replacing CO with CO<sub>2</sub>, and rebalancing the reaction accordingly, yielding the following global reaction: CH<sub>4</sub> + 2O<sub>2</sub>  $\rightarrow$  CO<sub>2</sub> + 2H<sub>2</sub>O. A parametric analysis of the Arrhenius terms in Eq. (9) revealed that adjusting the temperature exponent  $\beta$  allows for tuning the ignition delay without significantly altering the adiabatic flame temperature across different mixture compositions and pressures.

Table 2: Set of chemical reactions for the WD-Andersen two-step mechanism. The activation energy,  $E_a$ , is expressed in cal/mol,  $\beta$  is a dimensionless parameter, while reference units for A are cm, mol, and s, with the actual unit depending on the reaction order.

Reactions	$\boldsymbol{A}$	$\boldsymbol{\beta}$	$E_{\mathrm{a}}$	Orders
$CH_4 + \frac{3}{2}O_2 \rightarrow CO + 2H_2O$	$1.59 \times 10^{13}$	0	$47.8 \times 10^{3}$	$[CH_4]^{0.7}[O_2]^{0.8}$
$CO + \frac{1}{2}O_2 \rightarrow CO_2$	$3.98 \times 10^{8}$	0	$10.0\times10^3$	$[CO][O_2]^{0.25}[H_2O]^{0.5}$
$CO_2 \rightarrow CO + \frac{1}{2}O_2$	$6.16\times10^{13}$	-0.97	$78.4 \times 10^3$	$[CO_2][O_2]^{-0.25}[H_2O]^{0.5}$

## 4. Results and Discussion

# 4.1 Ignition Delay Bounds for Instability Prediction

To evaluate the influence of ignition delay on the prediction of combustion instability, a parametric analysis was conducted by varying the temperature exponent  $\beta$  in the Arrhenius expression of the simplified global mechanism. This analysis aimed to identify the ignition delay thresholds beyond which the OSK model fails to reproduce the expected unstable combustion behavior. Notably, setting  $\beta = 0$ , consistent with the original WD-Andersen formulation, resulted in an ignition delay curve nearly identical to that of the parent mechanism, indicating that the first reaction is mainly responsible for this parameter. Positive values of  $\beta$  led to a decrease in ignition delay, while negative values caused it to increase. By discarding configurations where the initial pressure oscillations decayed to a steady-state, failing to trigger instability, the resulting stability bounds are presented in Fig. 6. The upper and lower boundaries correspond to  $\beta = -0.55$  and  $\beta = -0.1$ , respectively.

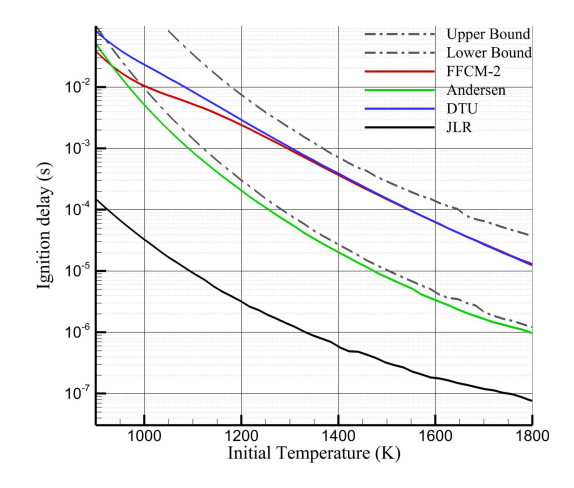


Figure 6: Ignition delay for different chemical mechanisms, with stability boundaries for the OSK mechanism (grey curves).

The identified bounds define a stability range centered around the ignition delays predicted by the DTU and FFCM-2 reference mechanisms. Since these reference curves lie closer to the upper bound, this suggests a tendency of reduced-order models to underestimate ignition delay. As previously noted by Andersen et al.,<sup>31</sup> this underestimation may arise from the inability of simplified models to capture the slow radical build-up that leads to ignition. Interestingly, although the WD-Andersen model successfully reproduces the unstable behavior, as shown in the previous section, it falls just below the lower stability limit, predicting an ignition delay shorter than the minimum threshold for the OSK mechanism. This suggests that each chemical mechanism, due to its specific set of reactions, species, and kinetic parameters, defines its own window within which combustion instability can be reliably reproduced. As the mechanism becomes more detailed and physically representative, this range may widen. This also suggests that, while ignition delay appears to play an important role in simulations of thermoacoustic combustion instability, other aspects of combustion modeling also deserve investigation. These, however, lie beyond the scope of the present study and are planned for future work. Nonetheless, the failure of the JLR mechanism to reproduce the test case self-sustained

behavior, suggests that substantial underestimation of ignition delay (up to three orders of magnitude in this case), cannot be compensated by increased model fidelity and complexity alone.

The phenomenology associated with out-of-boundary values of  $\beta$  for the OSK mechanism is illustrated through two representative cases. The first case features a temperature exponent  $\beta = -0.7$ , referred to as "OSK:  $\beta = -0.7$ ", corresponding to an ignition delay exceeding the upper boundary. The second case, with  $\beta = 0.4$  ("OSK:  $\beta = 0.4$ "), corresponds instead to an ignition delay below the lower boundary. The variation of ignition delay for "OSK:  $\beta = -0.7$ " and "OSK:  $\beta = 0.4$ " is shown in Fig. 7. The pressure signals for the out-of-bound OSK cases, sampled near the

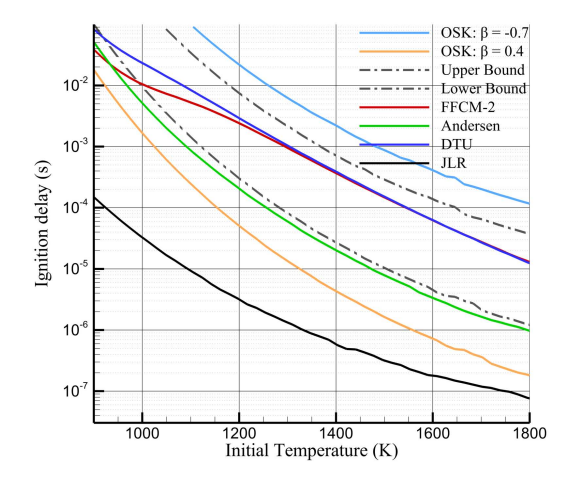
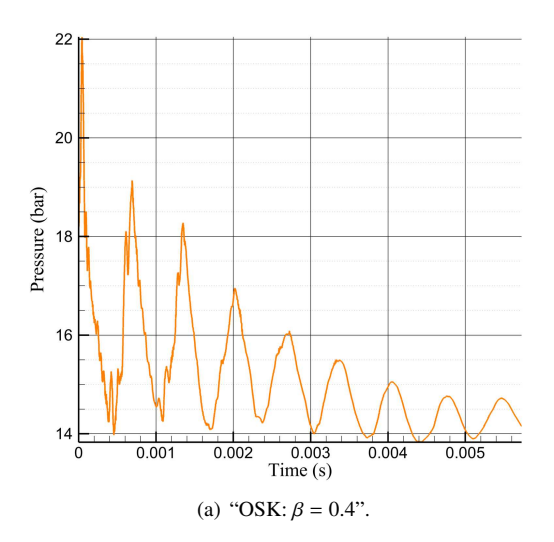


Figure 7: Ignition delay for different chemical mechanisms, including "OSK:  $\beta = -0.7$ " and "OSK:  $\beta = 0.4$ ", along with stability boundaries for the OSK mechanism (grey curves).

faceplate, are shown in Fig. 8. In both cases, a similar pattern of damped pressure oscillations is observed, featuring a rapid reduction in amplitude toward steady-state conditions. This indicates that neither mechanism is able to capture the self-excited behavior of the investigated test case. However, despite their similar outcomes, the underlying dynamics differ significantly, reflecting two fundamentally distinct phenomenologies.



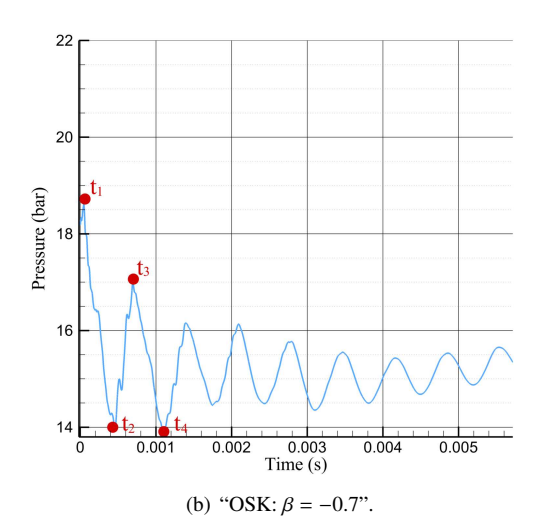


Figure 8: Pressure signals, sampled near the faceplate, for the out-of-bound OSK chemical mechanisms.

For the "OSK:  $\beta = 0.4$ " mechanism, the observed dynamics closely resembles that of the JLR, discussed in the previous section. Specifically, this faster mechanism leads to a fully ignited oxidizer-fuel interface anchored at the recess exit, mirroring the phenomenology previously shown for the JLR in Fig. 4. For the "OSK:  $\beta = -0.7$ " mechanism, instead, combustion remains largely confined within the chamber, as shown in Fig. 9, which illustrates temperature distributions at four consecutive time instants (corresponding to the red circles in the pressure signal of Fig. 8(b)). In this case, the longer ignition delay leads to a less reactive combustion process, increasing the thermoacoustic space/time lag. This shift causes the timing of key acoustic events to become misaligned with respect to the

chamber natural frequencies. This misalignment leads to the damping of pressure oscillations. As the resulting pressure perturbations become progressively less disruptive, their influence on the generation and release of fuel pockets is reduced, ultimately favoring a more continuous combustion process. It is interesting to note that the reasons behind the stability of these two OSK mechanisms differ: for  $\beta = 0.4$ , the stability is mainly due to hydrodynamic effects, whereas for  $\beta = -0.7$ , it is more closely related to the timing of thermoacoustic phenomena.

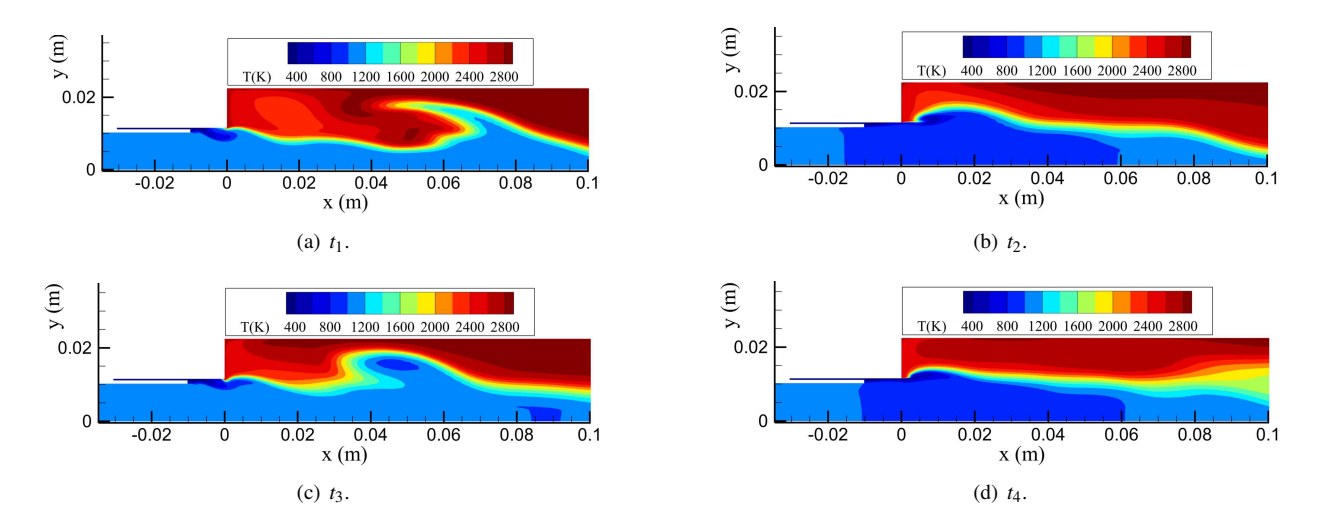


Figure 9: Temperature distributions at two consecutive cycle maxima and minima using the "OSK:  $\beta = -0.7$ " mechanism.

## 4.2 Effects of Ignition Delay on Unstable Configurations

The OSK mechanism has been able to reproduce the unstable behavior of the selected test case by tuning its ignition delay to remain within the stability boundaries identified in the previous section (see Fig. 6). To investigate how this parameter influences the predicted limit cycle and overall combustion dynamics, three representative OSK configurations have been considered. The first configuration, with a temperature exponent of  $\beta = -0.2$ , results in an ignition delay close to the lower boundary and is referred to as "Fast". The second, with  $\beta = -0.5$ , corresponds to an ignition delay near the upper boundary and is therefore labeled "Slow". The third, denoted as "Medium", is defined by  $\beta = -0.4$  and yields an ignition delay closely aligned with that of the DTU and FFCM-2 reference mechanisms. The ignition delays for these three configurations are shown in Fig. 10.

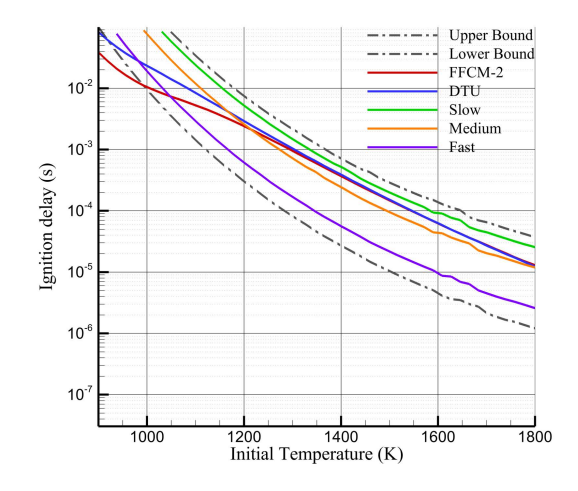


Figure 10: Ignition delay for the "Fast", "Medium", and "Slow" chemical mechanisms.

The limit cycle dominant frequencies and peak-to-peak amplitudes predicted employing these three OSK configurations are reported in Table 3, compared with the experimental data from.<sup>3</sup> Peak-to-peak values are shown for two distinct numerical probes. The first one, labeled "Probe-1", is positioned near the faceplate, 3.8 cm along the domain

longitudinal axis, while the second one, "Probe-2", is located near the nozzle entrance at 36.8 cm. Additionally, Fig. 11 presents the pressure signals sampled near the faceplate for each of the three mechanisms, along with their corresponding Fourier-transforms. A clear trend emerges in the predicted limit cycle frequencies. As the ignition delay increases, the oscillation frequency decreases, with differences in the dominant mode reaching up to 10%. This is particularly evident in the Fourier-transform results shown in Fig. 11(d), where, despite the similar spectral shapes across the different mechanisms, the peak frequencies consistently shift towards lower values from the "Fast" to the "Slow" OSK configuration. Similarly, the peak-to-peak amplitude of the limit cycle also exhibits a clear pattern, increasing with longer ignition delays. An increase of up to 49% is observed between the "Fast" and "Slow" mechanisms, based on the probe located near the nozzle entrance.

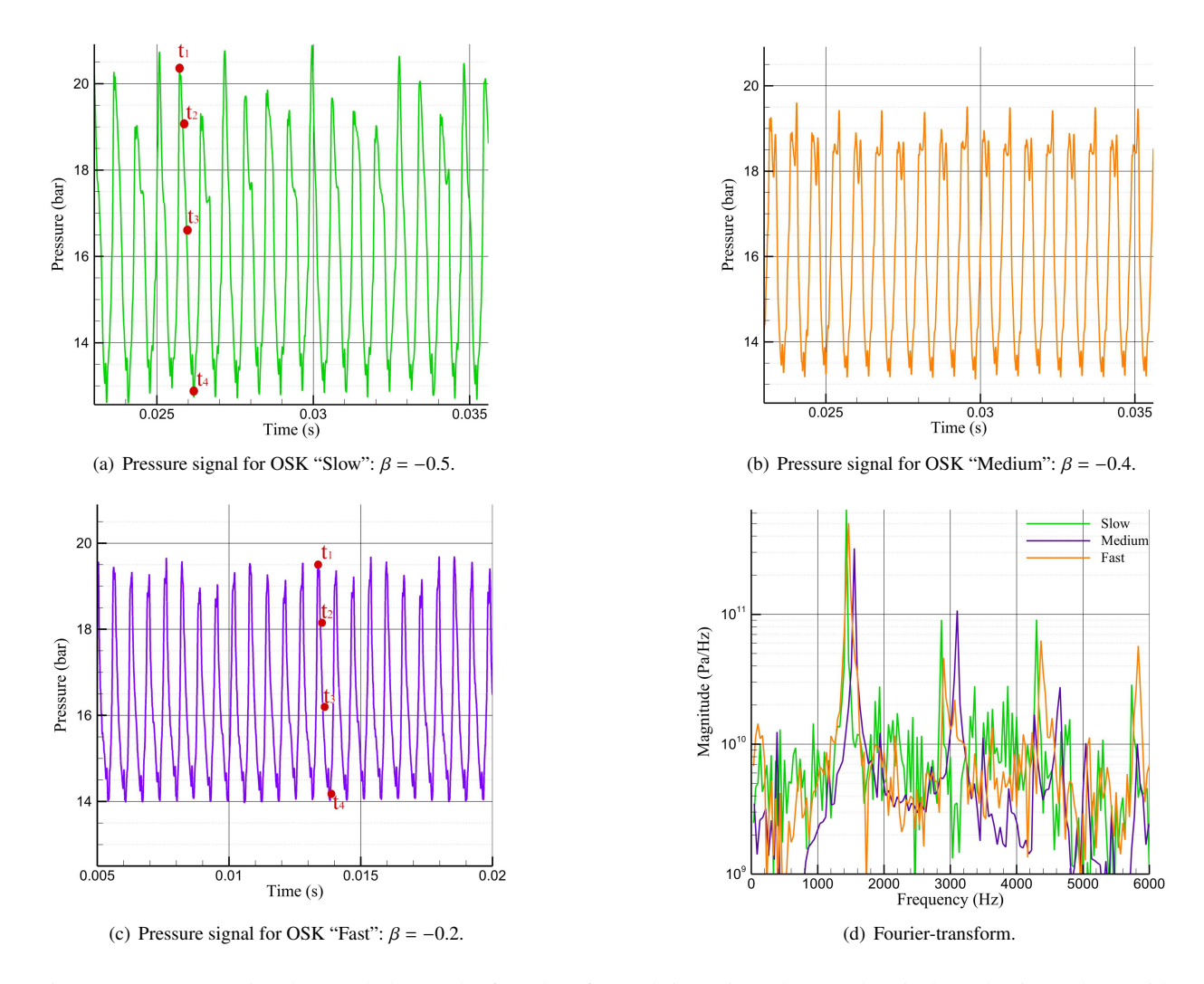


Figure 11: Pressure signals sampled near the faceplate for each investigated OSK chemical mechanism, along with their corresponding Fourier-transform.

Table 3: Comparison between model results and experimental data<sup>3</sup> for the dominant limit cycle frequency, f, and the peak-to-peak amplitude,  $p'_{\text{ptp}}$ .

	f (Hz)	Error $(\Delta f\%)$	Probe-1: $p'_{ptp}$ (bar)	Probe-2: $p'_{\text{ptp}}$ (bar)	Probe-2: Error $\left(\Delta p'_{ exttt{ptp}}\% ight)$
Experimental	1327	_	4.63	6.32	_
Fast	1561	17.6	4.48	5.13	18.8
Medium	1454	9.57	4.81	6.80	7.59
Slow	1420	7.01	5.83	7.65	21.04

To relate the observed changes in frequency and amplitude across chemical models to variations in ignition de-

lay, the two extreme cases, namely the "Fast" and the "Slow" configurations, are compared from a phenomenological perspective to identify which physical processes are most sensitive to this chemical parameter. Figure 12 presents a comparison of a single limit cycle period for the two mechanisms, showing temperature distributions at pressure maxima and minima, as well as two intermediate time instants. Observing Fig. 12, one of the most distinctive differences

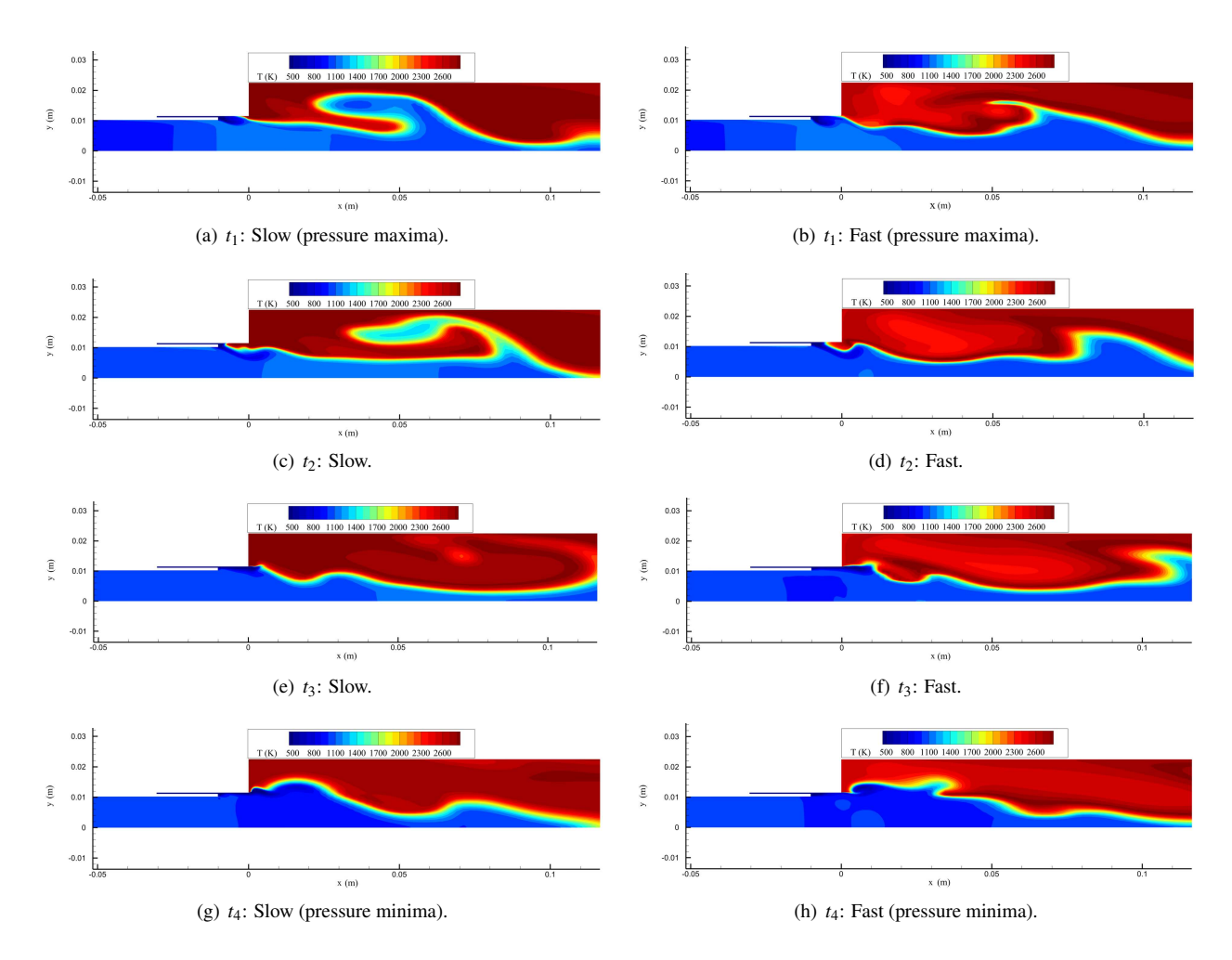


Figure 12: Temperature distributions at four time instants within a limit cycle period for the "Slow" and "Fast" chemical mechanisms (time instants highlighted as red dots in the pressure signals of Fig. 11).

between the two mechanisms is the extent of the vortical structure that forms at the fuel-oxidizer interface due its interaction with chamber pressure waves, which is the most evident at time  $t_1$ , Figs. 12(a) and 12(b). In the "Slow" mechanism, this structure appears significantly larger. This is attributed to the stronger pressure oscillations and to the delayed ignition of the mechanism, which leaves a larger fraction of the propellant unburned up to that point in the chamber. As a result, the pressure wave is able to stretch the interface more effectively, entraining a larger portion of oxidizer from the core flow into the recirculating region. At time  $t_2$  (Figs. 12(c)–12(d)) and  $t_3$  (Figs. 12(e)–12(f)), the "Slow" mechanism continues to ignite propellant within the entrained region. In contrast, for the "Fast" mechanism, the perturbed propellant interface is not only significantly smaller than in the "Slow" case at time  $t_1$ , but it has also already been consumed by combustion between time  $t_1$  and  $t_2$ . This rapid disappearance of the structure is attributed to the shorter ignition delay of the mechanism, which results in a more reactive combustion process. The observed differences play a key role in linking ignition delay to the observed variations in oscillation frequency between the investigated chemical mechanisms. This behavior can also be deduced observing Fig. 13, which shows the one-dimensional, cycleaveraged heat release distribution for each chemical mechanism. It is clear that the "Slow" configuration exhibits a peak region more distributed along the chamber axis, with a lower initial value and slope, reflecting a slower development of the flame. As a consequence, the space/time lag of the thermoacoustic cycle for this configuration increases. Due to the slower flame response and reduced combustion reactivity, more time is required for the system to generate a thermal response to acoustic perturbations. The result is a longer feedback loop period, which ultimately leads to lower oscillation frequencies. In contrast, the "Fast" mechanism exhibits a more abrupt combustion process, as evidenced

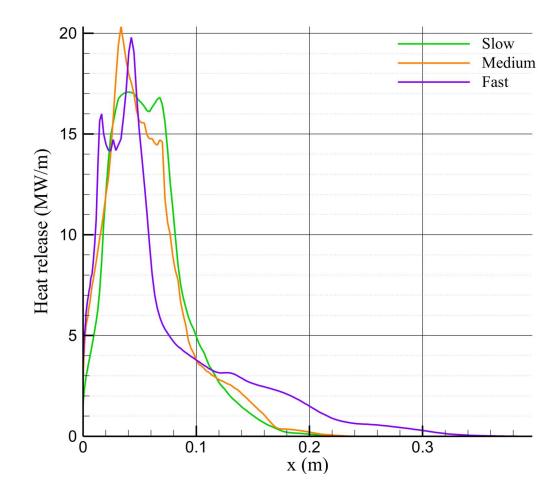


Figure 13: One-dimensional, cycle-averaged heat release distribution for each OSK chemical mechanism.

by the sharper peak in Fig. 13. This results in a reduced thermoacoustic spece/time lag and, consequently, to a shorter thermoacoustic period (i.e., higher limit cycle frequency).

Addressing the effects of ignition delay variations on peak-to-peak amplitude is more challenging, despite the clear trend observed in Table 3 where an increase in amplitude was associated with an increasing ignition delay. A useful starting point is the heat release profiles of each chemical mechanism shown in Fig. 13. At first glance, one might expect the mechanism with the most abrupt combustion process to produce the highest oscillation amplitudes, while the mechanism with a broader and smoother heat release peak to yield lower amplitudes. This assumption seems reasonable, as sharp, unsteady heat release fluctuations are typically associated with stronger acoustic responses during thermoacoustic coupling. However, the observed trend is the opposite, as the mechanism with the broadest and and smallest heat release peak (i.e., the "Slow" mechanism) corresponds to the highest pressure oscillation amplitude, whereas the "Fast" mechanism exhibits the smallest amplitude. To explain this it is important to recall that thermoacoustic coupling alone is not sufficient to trigger or sustain combustion instabilities. As discussed in Section §1, high-frequency combustion instabilities arise from a dual coupling mechanism. Not only must a thermoacoustic feedback loop be present, but the timing of the key events in this feedback loop, particularly the generation of acoustic waves in response to unsteady heat release, must also be aligned with the natural acoustic modes of the chamber.

This correlation between thermal and acoustic events can be assessed using the classical Rayleigh Criterion, which states that combustion instability is promoted when pressure and heat release fluctuations are in phase, thus when unsteady heat release acts as a source of acoustic energy. Mathematically, this condition is expressed as:

$$\int_{\tau} \int_{V} p' \dot{q}' dV dt > 0 \tag{10}$$

where  $\tau$  is the reference period of the oscillations, V is the combustion chamber volume, and p',  $\dot{q}'$  denote the fluctuating components of pressure and heat release, respectively. In essence, the Rayleigh criterion quantifies the degree of constructive interaction between pressure and heat release fluctuations, serving as a measure of the system tendency to amplify or dampen acoustic oscillations. The results of this evaluation are presented in Fig. 14, which shows the spatial distribution of the integrand of Rayleigh's criterion in Eq. (10),  $(p' \cdot q')$ , commonly referred to as "Rayleigh index", for both the "Slow" and "Fast" mechanisms. The selected time instants match those used in Fig. 12, corresponding to the reference points highlighted in the pressure signals of Fig. 11.

The figure shows that, for the "Slow" mechanism, the Rayleigh index remains consistently positive over large regions of the flow field, especially during pressure maxima. This indicates a sustained and constructive coupling between thermal and acoustic phenomena, suggesting that the arrival of compression waves is well aligned with zones of intense heat release. Notably, negative values of the Rayleigh index are mostly absent, implying a lack of significant dissipative interactions. In contrast, the "Fast" mechanism displays a smaller region where constructive thermoacoustic interaction occurs, indicating that thermal and acoustic events are slightly out of phase. Additionally, localized zones of negative Rayleigh index appear, highlighting the presence of destructive interactions that act as dissipative mechanisms due to this phase shift. These observations suggest that the variation in thermoacoustic space/time lag, caused by differences in ignition delay between the two mechanisms, directly influences the alignment between heat release fluctuations, driven by the thermoacoustic feedback loop, and the passage of pressure waves, which are determined by the chamber natural resonance frequencies. In the investigated CVRC test case, as the ignition delay decreases, this

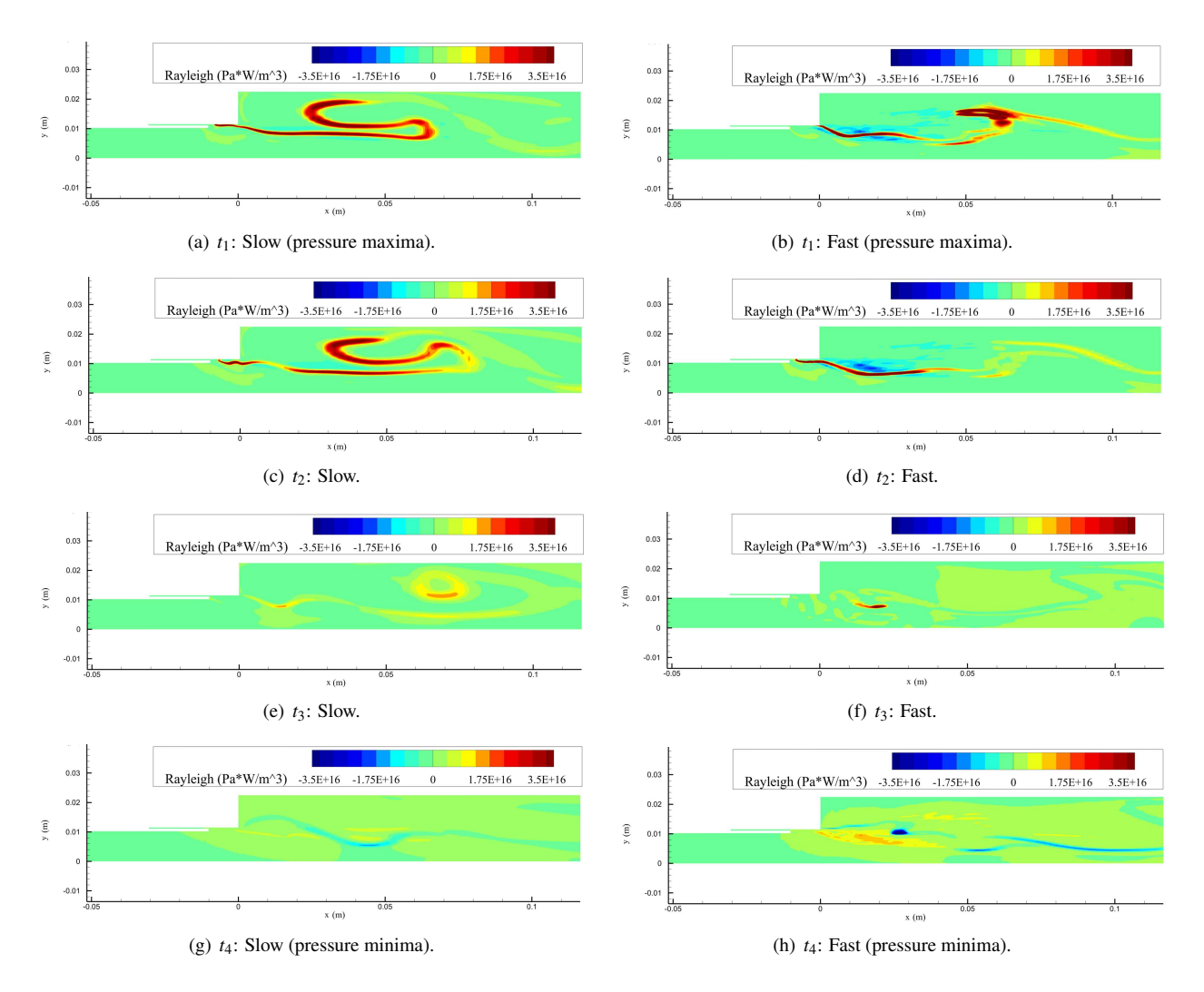


Figure 14: Distribution of Rayleigh index,  $(p' \cdot q')$ , for the "Slow" and "Fast" chemical mechanisms (time frames are the same as in Fig. 12).

alignment weakens, leading to a less effective coupling between thermal and acoustic events, ultimately leading to a reduction in peak-to-peak amplitude. To quantitatively support this interpretation, integrating the Rayleigh index over the entire domain and over three full limit cycle periods yields a Rayleigh criterion value for the "Slow" mechanism approximately 115% times higher than that of the "Fast" mechanism. The "Medium" OSK mechanism further corroborates this trend, producing a Rayleigh criterion value that lies between those of the "Slow" and "Fast" mechanisms. These results are also consistent with the stable behavior observed for the out-of-bounds "OSK:  $\beta = -0.7$ " mechanism, discussed in the previous section.

Looking at the comparison between the results and experimental data in Table 3, it is important to note that the obtained results align well with literature data. Specifically, the "Fast" combustion model, which features an ignition delay similar to the WD-Andersen model, as shown in Fig. 6, predicts limit cycle features that closely match those reported in previous studies. Notably, better alignment of the ignition delay with the more physically accurate values provided by the DTU and FFCM-2 mechanisms, achieved with the "Medium" OSK configuration, significantly improves the predictions. Despite using a heavily simplified global one-step chemical kinetics, the "Medium" configuration achieved remarkably small errors for the limit cycle frequency and the peak-to-peak amplitude, both dropping below 10% (9.6% frequency and 7.59% amplitude error), corresponding to an 8% improvement in frequency prediction and a 11% improvement in amplitude prediction compared to the "Fast" mechanism.

These results highlight the critical role of ignition delay in predicting combustion instabilities, even when employing simplified chemical models. The findings demonstrate that, in combustion instability analysis, chemical timescales can be more influential than the level of chemical detail, so that accurate predictions can still be achieved with simplified chemical mechanisms, greatly enhancing computational efficiency. The investigations presented here

provide a solid starting point for making physically-informed choices in chemical modeling, whether for high-fidelity CFD simulations or reduced-order modeling approaches.

## 5. Conclusions

In this work, the influence of combustion modeling, specifically ignition delay, on the prediction of thermoacoustic instabilities has been investigated using a two-dimensional axisymmetric URANS approach applied to the Continuously Variable Resonance Combustor (CVRC), a well-established test case exhibiting longitudinal combustion instabilities. Two chemical mechanisms, the Westbrook-Dryer model with Andersen correction (WD-Andersen) and the John-Lindstedt Recombination mechanism (JLR), both capable of reproducing key combustion observables such as heat release, temperature, and species composition, were assessed. Despite their comparable predictive capabilities in canonical chemical observables, they yielded markedly different results, with the JLR mechanism failing to capture the self-excited nature of the investigated CVRC configuration. The primary factor distinguishing their performance was identified to be ignition delay.

Based on this observation, the WD-Andersen mechanism, which successfully reproduced the unstable dynamics of the CVRC in agreement with literature results, was selected as a baseline for designing a simplified global one-step mechanism, referred to as "OSK". By systematically tuning its parameters, three OSK variants were generated, each characterized by a distinct ignition delay, thereby enabling a controlled investigation into its role in combustion instability prediction. Analysis of the resulting limit cycles revealed that ignition delay strongly influences both the oscillation frequency and amplitude. In particular, longer ignition delays resulted in lower limit cycle frequencies, a trend attributed to the increased space/time lag in the thermoacoustic feedback loop. This slower thermal response increases the duration of the thermoacoustic feedback period, thereby reducing the dominant frequency. A similar correlation was observed for oscillation amplitude, with longer ignition delays leading to higher peak-to-peak amplitudes. Evaluation of Rayleigh's criterion showed that, in the investigated test case, increased ignition delay with respect to the reference WD-Andersen mechanism enhances the constructive coupling between heat release fluctuations and pressure waves, due to an improved phase alignment between the key events of the thermoacoustic loop and the natural frequencies of the chamber.

Notably, calibrating the ignition delay of the simplified OSK mechanism to partially match reference values from batch reactor simulations using detailed models significantly improved its predictive accuracy, yielding errors with respect to experimental data below 10% for both oscillation frequency and amplitude, specifically a 9.6% error for the first observable and a 7.59% error for the second. This demonstrates that in the context of combustion instability prediction, chemical timescales such as ignition delay may be more critical than the level of chemical detail. A physically informed choice of simplified mechanisms can thus yield reliable predictions at significantly reduced computational cost, particularly valuable for both high-fidelity CFD and reduced-order modeling.

Nonetheless, while ignition delay has proven to be a dominant parameter in this study, further investigation into the influence of additional chemical properties is warranted. Future work will extend this approach to other unstable regimes and propellant combinations, and will explore how variations in other chemical kinetics parameters influence combustion instability predictions.

# Acknowledgements

Support from Project ECS 0000024 Rome Technopole, - CUP B83C22002820006, NRP Mission 4 Component 2 Investment 1.5, Funded by the European Union - "NextGenerationEU" is acknowledged.

#### References

- [1] Heister, S. D., Anderson, W. E., Pourpoint, T. L., and Cassady, R. J., *Rocket propulsion*, Vol. 47, Cambridge University Press, 2019, 10.1017/9781108381376.
- [2] Oefelein, J. C. and Yang, V., "Comprehensive review of liquid-propellant combustion instabilities in F-1 engines," *Journal of Propulsion and Power*, Vol. 9, No. 5, 1993, pp. 657–677, 10.2514/3.23674.
- [3] Yu, Y. C., Sisco, J. C., Rosen, S., Madhav, A., and Anderson, W. E., "Spontaneous Longitudinal Combustion Instability in a Continuously-Variable Resonance Combustor," *Journal of Propulsion and Power*, Vol. 28, No. 5, 2012, pp. 876–887, 10.2514/1.B34308.

- [4] Yu, Y., Sisco, J., Anderson, W., and Sankaran, V., "Examination of Spatial Mode Shapes and Resonant Frequencies Using Linearized Euler Solutions," *37th AIAA Fluid Dynamics Conference and Exhibit*, Miami, FL, USA, 2007, AIAA 2007-3999, 10.2514/6.2007-3999.
- [5] Yu, Y., O'Hara, L., Sisco, J., and Anderson, W., "Experimental Study of High-Frequency Combustion Instability in a Continuously Variable Resonance Combustor (CVRC)," 47th AIAA Aerospace Sciences Meeting including The New Horizons Forum and Aerospace Exposition, Orlando, FL, USA, 2009, AIAA 2009-234, 10.2514/6.2009-234.
- [6] Gröning, S., Hardi, J. S., Suslov, D., and Oschwald, M., "Injector-Driven Combustion Instabilities in a Hydrogen/Oxygen Rocket Combustor," *Journal of Propulsion and Power*, Vol. 32, No. 3, 2016, pp. 560–573, 10.2514/1.B35768.
- [7] Pomeroy, B. and Anderson, W., "Transverse Instability Studies in a Subscale Chamber," *Journal of Propulsion and Power*, Vol. 32, No. 4, 2016, pp. 939–947, 10.2514/1.B35763.
- [8] Martin, J., Armbruster, W., Stützer, R., Suslov, D., Hardi, J., and Oschwald, M., "Flame dynamics of an injection element operated with LOX/H2, LOX/CNG and LOX/LNG in a sub- and supercritical rocket combustor with large optical access," *International Journal of Spray and Combustion Dynamics*, Vol. 15, No. 3, 2023, pp. 147–165, 10.1177/17568277231172302.
- [9] Hardi, J., Oschwald, M., and Dally, B., "Flame response to acoustic excitation in a rectangular rocket combustor with LOX/H2 propellants," *CEAS Space Journal*, Vol. 2, No. 4, 2011, pp. 41–49, 10.1007/s12567-011-0020-z.
- [10] Harvazinski, M. E., Huang, C., Sankaran, V., Feldman, T. W., Anderson, W. E., Merkle, C. L., and Talley, D. G., "Coupling between hydrodynamics, acoustics, and heat release in a self-excited unstable combustor," *Physics of Fluids*, Vol. 27, No. 4, 04 2015, pp. 045102, 10.1063/1.4916673.
- [11] Srinivasan, S., Ranjan, R., and Menon, S., "Flame Dynamics During Combustion Instability in a High-Pressure, Shear-Coaxial Injector Combustor," *Flow, Turbulence and Combustion*, Vol. 94, No. 1, 2015, pp. 237–262, 10.1007/s10494-014-9569-x.
- [12] Urbano, A., Selle, L., Staffelbach, G., Cuenot, B., Schmitt, T., Ducruix, S., and Candel, S., "Exploration of combustion instability triggering using Large Eddy Simulation of a multiple injector liquid rocket engine," *Combustion and Flame*, Vol. 169, 2016, pp. 129–140, 10.1016/j.combustflame.2016.03.020.
- [13] Nguyen, T. M. and Sirignano, W. A., "Spontaneous and Triggered Longitudinal Combustion Instability in a Single-Injector Liquid-Rocket Combustor," *AIAA Journal*, Vol. 57, No. 12, 2019, pp. 5351–5364, 10.2514/1.J057743.
- [14] Xiong, J., Liu, F., and Sirignano, W. A., "Combustion Simulation of 82-Injector Rocket Engine," *AIAA Journal*, Vol. 60, No. 8, 2022, pp. 4601–4613, 10.2514/1.J061255.
- [15] Smith, R., Ellis, M., Xia, G., Sankaran, V., Anderson, W., and Merkle, C. L., "Computational Investigation of Acoustics and Instabilities in a Longitudinal-Mode Rocket Combustor," *AIAA Journal*, Vol. 46, No. 11, 2008, pp. 2659–2673, 10.2514/1.28125.
- [16] Sirignano, W. A. and Popov, P. P., "Two-Dimensional Model for Liquid-Rocket Transverse Combustion Instability," *AIAA Journal*, Vol. 51, No. 12, 2013, pp. 2919–2934, 10.2514/1.J052512.
- [17] Crocco, L. and Cheng, S.-I., *Theory of Combustion Instability in Liquid Propellant Rocket Motors*, Princeton University, Princeton, NJ, USA, 1956, https://apps.dtic.mil/sti/pdfs/AD0688924.pdf.
- [18] Frezzotti, M. L., Nasuti, F., Huang, C., Merkle, C. L., and Anderson, W. E., "Quasi-1D modeling of heat release for the study of longitudinal combustion instability," *Aerospace Science and Technology*, Vol. 75, 2018, pp. 261–270, 10.1016/j.ast.2018.02.001.
- [19] D'Alessandro, S., Frezzotti, M. L., Favini, B., and Nasuti, F., "Driving Mechanisms in Low-Order Modeling of Longitudinal Combustion Instability," *Journal of Propulsion and Power*, Vol. 39, No. 5, 2023, pp. 754–764, 10.2514/1.B39048.
- [20] Zolla, P. M., Montanari, A., D'Alessandro, S., Pizzarelli, M., Nasuti, F., Pellegrini, R. C., and Cavallini, E., "Low-order modeling approach for the prediction of transverse combustion instabilities in multi-injector engines," *CEAS Space Journal*, Vol. 16, No. 6, 2024, pp. 635–657, 10.1007/s12567-024-00538-y.

- [21] Montanari, A., Zolla, P. M., D'Alessandro, S., Pizzarelli, M., Nasuti, F., Pellegrini, R. C., Cavallini, E., et al., "Sensitivity study on a low order model for the analysis of tranverse combustion instability," *10th European Conference for Aeronautics and Space Sciences*, Lausanne, Switzerland, 2023, 10.13009/EUCASS2023-506.
- [22] Zolla, P. M., Montanari, A., D'Alessandro, S., Pizzarelli, M., and Nasuti, F., "Low Order Modeling of Combustion Instability Using a Hybrid Real/Ideal Gas Mixture Model," 9th European Conference for Aeronautics and Space Sciences, Lille, France, 2022, https://www.eucass.eu/component/docindexer/?task=download&id=6621.
- [23] Zolla, P. M., Montanari, A., Grossi, M., Nasuti, F., Armbruster, W., Börner, M., and Hardi, J., "Low-Order Modeling of Combustion Instability: A Comprehensive Analysis of the BKD Test Case," AIAA SciTech Forum, Orlando, FL, USA, 2024, AIAA 2024-0150, 10.2514/6.2024-0150.
- [24] Zolla, P. M., Prediction and analysis of high-frequency combustion instabilities in liquid rocket engines using low-order modeling, Ph.D. thesis, Università degli Studi di Roma "La Sapienza", 2025, 10.13140/RG.2.2.33881.84326.
- [25] Sutton, K. and Gnoffo, P., "Multi-component diffusion with application to computational aerothermodynamics," 7th AIAA/ASME Joint Thermophysics and Heat Transfer Conference, Albuquerque, NM, USA, 1998, AIAA 1998-2575, 10.2514/6.1998-2575.
- [26] Gordon, S. and McBride, B. J., "Computer Program for Calculation of Complex Chemical Equilibrium Compositions and Applications," Tech. Rep. NASA-RP-1311, National Aeronautics and Space Administration, Washington, USA, 1996, https://ntrs.nasa.gov/citations/19950013764.
- [27] SPALART, P. and ALLMARAS, S., "A one-equation turbulence model for aerodynamic flows," 30th Aerospace Sciences Meeting and Exhibit, Reno, NV, USA, 1992, AIAA 1992-439, 10.2514/6.1992-439.
- [28] Batten, P., Clarke, N., Lambert, C., and Causon, D. M., "On the Choice of Wavespeeds for the HLLC Riemann Solver," *SIAM Journal on Scientific Computing*, Vol. 18, No. 6, 1997, pp. 1553–1570, 10.1137/S1064827593260140.
- [29] Harvazinski, M. E., Gejji, R., Talley, D. G., Orth, M. R., Anderson, W. E., and Pourpoint, T. L., "Modeling of Transverse Combustion Instability," *AIAA Scitech Forum*, San Diego, CA, USA, 2019, AIAA 2019-1732, 10.2514/6.2019-1732.
- [30] Liu, Y., Liu, P., Wang, Z., Ao, W., Xu, G., and Guan, Y., "Numerical investigation of combustion instability in a liquid rocket engine: Interaction effect between hydrodynamics and acoustic mode," *Aerospace Science and Technology*, Vol. 143, 2023, pp. 108711, 10.1016/j.ast.2023.108711.
- [31] Andersen, J., Rasmussen, C. L., Giselsson, T., and Glarborg, P., "Global Combustion Mechanisms for Use in CFD Modeling under Oxy-Fuel Conditions," *Energy & Fuels*, Vol. 23, No. 3, 2009, pp. 1379–1389, 10.1021/ef8003619.
- [32] Betti, B., Bianchi, D., Nasuti, F., and Martelli, E., "Chemical Reaction Effects on Heat Loads of CH4/O2 and H2/O2 Rockets," *AIAA Journal*, Vol. 54, No. 5, 2016, pp. 1693–1703, 10.2514/1.J054606.
- [33] Frezzotti, M. L., Nasuti, F., Huang, C., and Anderson, W. E., "Extraction of response function from numerical simulations and their use for longitudinal combustion intsbility modeling," *55th AIAA Aerospace Sciences Meeting*, Grapevine, TX, USA, 2017, AIAA 2017-1338, 10.2514/6.2017-1338.
- [34] Sardeshmukh, S. V., Heister, S. D., and Anderson, W. E., "Prediction of Combustion Instability with Detailed Chemical Kinetics," *53rd AIAA Aerospace Sciences Meeting*, Kissimmee, FL, USA, 2015, AIAA 2015-1826, 10.2514/6.2015-1826.
- [35] Goodwin, D. G., Speth, R. L., Moffat, H. K., and Weber, B. W., "Cantera: An Object-oriented Software Toolkit for Chemical Kinetics, Thermodynamics, and Transport Processes," 2021, Zenodo, 10.5281/zenodo.4527812.
- [36] Hashemi, H., Christensen, J. M., Gersen, S., Levinsky, H., Klippenstein, S. J., and Glarborg, P., "High-pressure oxidation of methane," *Combustion and Flame*, Vol. 172, 2016, pp. 349–364, 10.1016/j.combustflame.2016.07.016.
- [37] Zhang, Y., Dong, W., Vandewalle, L., Xu, R., Smith, G., and Wang, H., "Foundational Fuel Chemistry Model Version 2.0 (FFCM-2)," 2023, https://web.stanford.edu/group/haiwanglab/FFCM2.